

A temperature condensation trend in the debris-disk binary system ζ^2 Ret

C. Saffe^{1,2,6}, M. Flores^{1,6}, M. Jaque Arancibia^{1,6}, A. Buccino^{3,4,6} and E. Jofré^{5,6}

¹ Instituto de Ciencias Astronómicas, de la Tierra y del Espacio (ICATE-CONICET), C.C 467, 5400, San Juan, Argentina. e-mail: csaffe, mflores, mjaque@icate-conicet.gob.ar

² Universidad Nacional de San Juan (UNSJ), Facultad de Ciencias Exactas, Físicas y Naturales (FCEFyN), San Juan, Argentina.

³ Instituto de Astronomía y Física del Espacio (IAFE-CONICET), Buenos Aires, Argentina. e-mail: abuccino@iafe.uba.ar

⁴ Departamento de Física, Facultad de Ciencias Exactas y Naturales (FCEN), Universidad de Buenos Aires (UBA), Buenos Aires, Argentina.

⁵ Observatorio Astronómico de Córdoba (OAC), Laprida 854, X5000BGR, Córdoba, Argentina. e-mail: emiliano@oac.uncor.edu

⁶ Consejo Nacional de Investigaciones Científicas y Técnicas (CONICET), Argentina

Received xxx, xxx ; accepted xxxx, xxxx

ABSTRACT

Context. Detailed abundance studies have reported different trends between samples of stars with and without planets, possibly related to the planet formation process. Whether these differences are still present between samples of stars with and without debris disk is still unclear.

Aims. We explore condensation temperature T_c trends in the unique binary system ζ^1 Ret - ζ^2 Ret, to determine whether there is a depletion of refractories, which could be related to the planet formation process. The star ζ^2 Ret hosts a debris disk which was detected by an IR excess and confirmed by direct imaging and numerical simulations, while ζ^1 Ret does not present IR excess nor planets. These characteristics convert ζ^2 Ret in a remarkable system, where their binary nature together with the strong similarity of both components allow us, for the first time, to achieve the highest possible abundance precision in this system.

Methods. We carried out a high-precision abundance determination in both components of the binary system via a line-by-line, strictly differential approach. First, we used the Sun as a reference and then we used ζ^2 Ret. The stellar parameters T_{eff} , $\log g$, [Fe/H] and v_{turb} were determined by imposing differential ionization and excitation equilibrium of Fe I and Fe II lines, with an updated version of the program FUNDPAR, together with plane-parallel local thermodynamic equilibrium (LTE) ATLAS9 model atmospheres and the MOOG code. Then, we derived detailed abundances of 24 different species with equivalent widths and spectral synthesis with the MOOG program. The chemical patterns were compared with the solar-twins T_c trend of Meléndez et al. (2009), and then mutually between both stars of the binary system. The rocky mass of depleted refractory material was estimated according to Chambers (2010).

Results. The star ζ^1 Ret resulted slightly more metal rich than ζ^2 Ret by ~ 0.02 dex. In the differential calculation of ζ^1 Ret using ζ^2 Ret as reference, the abundances of the refractory elements resulted higher than the volatile elements, and the trend of the refractory elements with T_c showed a positive slope. These facts together show a lack of refractory elements in ζ^2 Ret (a debris-disk host) relative to ζ^1 Ret. The T_c trend would be in agreement with the proposed signature of planet formation (Meléndez et al. 2009) rather than possible Galactic Chemical Evolution or age effects, which are largely diminished here. Then, following the interpretation of Meléndez et al. (2009), we propose an scenario in which the refractory elements depleted in ζ^2 Ret are possibly locked-up in the rocky material that orbits this star and produce the debris disk observed around this object. We estimated a lower limit of $M_{rock} \sim 3 M_\oplus$ for the rocky mass of depleted material, which is compatible with a rough estimation of $3\text{-}50 M_\oplus$ of a debris disk mass around a solar-type star (Krivov et al. 2008).

Key words. Stars: abundances – Stars: planetary systems – Stars: binaries – Stars: individual: ζ^1 Ret (= HD 20766), ζ^2 Ret (= HD 20807)

1. Introduction

Meléndez et al. (2009, hereafter M09) showed that the Sun is deficient in refractory elements relative to volatile elements when compared to the mean abundances of 11 solar twins. They also found that the abundance differences correlate strongly with the condensation temperature T_c , which is interpreted by the authors as a possible signature of terrestrial planet formation in the Solar System. They suggested that the refractory elements ($T_c > 900$ K) depleted in the solar photosphere are locked up in terrestrial planets and rocky material at the time of star and planet formation. In a follow-up study, Ramírez et al. (2010, hereafter R10) confirmed their findings. Gonzalez et al. (2010) and Gonzalez (2011) also found that most metal-rich exoplanet host

(EH) stars have the most negative trends. These results indicate that the depletion of refractory elements in a photosphere is a consequence of both terrestrial and giant planet formation. If this hypothesis is correct, stars with planetary systems like ours may be identified through a very detailed inspection of the chemical composition.

Debris disks orbiting main-sequence stars are observationally characterized by an infrared excess over the normal photospheric fluxes of their host stars (see e.g. Aumann et al. 1984; Mannings & Barlow 1998; Habing et al. 2001; Bryden et al. 2006; Beichman et al. 2006). The excess is produced by the presence of dust in the disk which is attributed to the collisions of larger rocky bodies (see e.g. the reviews of

Wyatt 2008; Moro-Martin 2013; Matthews et al. 2014, and references therein). The existence of these dusty disks is confirmed in some cases by direct imaging, starting with the first β Pictoris image by Smith & Terrile (1984) and then followed by other examples (see e.g. Krist et al. 2005; Vandenbussche et al. 2010; Soumer et al. 2014; Currie et al. 2015). Maldonado et al. (2015, hereafter MA15) compared T_c trends in a sample of stars with debris disks and stars with neither debris nor planets, and found no statistical difference between them. In other words, they do not detect a possible lack of refractory elements in debris disk stars when compared to stars without disks. The detection of a T_c trend is a challenging task that requires the highest possible precision in abundances, such as those obtained with the line-by-line differential technique (e.g. Bedell et al. 2014; Saffe et al. 2015). However, the sample of MA15 included 251 FGK stars spanning a range in T_{eff} of ~ 2000 K, which prevented the authors to perform a differential analysis, as they explained. In addition, the study of binary systems with similar components greatly diminishes other T_c effects such as the Galactic Chemical Evolution (GCE, González Hernández et al. 2013; Schuler et al. 2011a), the stellar age and a possible inner galactic origin of the planet hosts (e.g. Adibekyan et al. 2014), thanks to the common natal environment of the pair. MA15 showed that these effects are indeed present in their sample, suggesting that an evolutionary effect is present. Then, the study of binary systems with similar components presents important advantages aiming to detect a possible T_c trend related to the planet formation process (e.g. Tucci Maia et al. 2014; Saffe et al. 2015).

Up to now, to find a binary system (with similar components) where only one star hosts a debris disk is a very difficult task. Most of the IR surveys performed with the satellite Spitzer have been mainly focused on single main-sequence stars rather than multiple systems (e.g. Beichman et al. 2005; Rieke et al. 2005; Bryden et al. 2006; Su et al. 2006). Using Spitzer data, the location of the dust in a multiple system (i.e. circumstellar, circumbinary or both) could be determined only in very few cases (see e.g. Trilling et al. 2007). Rodriguez & Zuckerman (2012) showed that only $\sim 25\%$ of the debris disk stars in their sample of 112 main-sequence stars belong to multiple systems. The satellite Herschel overcome some of these difficulties, thanks to their greater sensitivity and spatial resolution. Different Herschel surveys such as SUNS, DEBRIS (Matthews et al. 2010; Phillips et al. 2010), and DUNES (Eiroa et al. 2010; Löhne et al. 2012; Eiroa et al. 2013) do include multiple systems in their samples. However, the circumstellar nature of the dust have been determined in few multiple systems (see e.g. Eiroa et al. 2013). Recently, Rodriguez et al. (2015) estimated a multiplicity of $\sim 42\%$ in the stars of the DEBRIS survey by using adaptive optics imaging. However, there is no physical data of many systems and most of them do not present similar components (see e.g. their Table 1). This shows how particular could be to find such kind of binary system.

As a part of the DUNES survey, Eiroa et al. (2010) discovered a resolved debris disk around the star ζ^2 Ret (= HD 20807), which is accompanied by the star ζ^1 Ret (= HD 20766). The projected distance between the stars is 3713 AU (Mason et al. 2001), while a Bayesian analysis of the proper motions indicates a very high probability (near 100%) that the pair is physically connected (Shaya & Olling 2011). This is an unique system for a number of reasons. The presence of a debris disk around ζ^2 Ret was detected through a mid-IR excess (Trilling et al. 2008; Eiroa et al. 2013), it was *confirmed* by direct imaging (Eiroa et al. 2010), and also supported by numerical simulations

(Faramaz et al. 2014). On the other hand, the companion ζ^1 Ret does not present IR excess using both Spitzer and Herschel observations (Bryden et al. 2006; Trilling et al. 2008; Eiroa et al. 2013). The spectral types of the binary components are very similar (G2 V + G1 V, as appear in the Hipparcos database) allowing a chemical comparison less dependent of the fundamental parameters of the stars. Both stars are also very similar to the Sun, being both solar-analogs. Also, there is no planet detected in this binary system (as we explain below), which is a condition for the sample of MA15. These characteristics shows that this is a remarkable binary system, an ideal case to test a possible T_c trend in stars with and without debris disks.

Using numerical simulations, Faramaz et al. (2014) suggested that the eccentric structure of the ζ^2 Ret debris disk could be caused by an eccentric ($e > 0.3$) planetary companion. However, both stars (ζ^1 and ζ^2) have been monitored by the Anglo-Australian Planet Search (AAPS) radial-velocity survey¹, while ζ^2 Ret was also included in the HARPS GTO planet search program (e.g. Sousa et al. 2008) giving no-planet detection. The AAPS survey allows to rule out a Saturn-mass ($0.3 M_{Jup}$) or a larger planet with a period range $P < 300$ days and eccentricity $0.0 < e < 0.6$ (Wittenmyer et al. 2010). The HARPS GTO survey suggests that there is no Jupiter-mass or a larger planet interior to ~ 5 –10 AU (Mayor et al. 2003). Although the radial-velocity surveys cannot completely rule out the presence of planets (such as e.g. long period perturbers or lower-mass planets), these stars form, to our knowledge, the only solar-like binary system with similar components where only one component hosts a debris disk (confirmed by direct imaging) and the presence of planets has not been confirmed yet.

Surprisingly, in this work we found a T_c trend between the components of this binary system i.e. a lack of refractory elements in a debris-disk star. We note that the MA15 statistical result does not exclude that T_c trends may be present in particular stars, such as the components of the ζ Ret system. The T_c trend would be in agreement with the proposed signature of planet formation (e.g. Meléndez et al. 2009; Ramírez et al. 2010) rather than possible GCE, age or evolutionary effects which are largely diminished here.

The abundances of the stars have been previously determined in the literature. However, there are some differences in the fundamental parameters derived for ζ^2 Ret. The reported metallicities vary from -0.16 dex to -0.36 dex (Maldonado et al. 2012; Allende Prieto et al. 2004) while $\log g$ vary between 4.41 dex and 4.64 dex (Bensby et al. 2014; Maldonado et al. 2012). These differences also encouraged this work, searching for a slight difference between the components of this binary system.

This work is organized as follows. In Section §2 we describe the observations and data reduction, while in Section §3 we present the stellar parameters and chemical abundance analysis. In Section §4 we show the results and discussion, and finally in Section §5 we highlight our main conclusions.

2. Observations and data reduction

Stellar spectra of ζ^1 Ret and ζ^2 Ret were obtained with the High Accuracy Radial velocity Planet Searcher (HARPS) spectrograph, attached to the La Silla 3.6m (ESO) telescope. The spectrograph was fed by a pair of fibres with an aperture of 1 arcsec on the sky, resulting a resolving power of $\sim 115000^2$. The

¹ <http://newt.phys.unsw.edu.au/~cgt/planet/Targets.html>

² <http://www.eso.org/sci/facilities/lasilla/instruments/harps/overview.html>

spectra were obtained from the ESO HARPS archive³, under the ESO program identification 072.C-0513(D).

The observations were taken on February, 4th 2004 with ζ^2 Ret observed immediately after ζ^1 Ret, using the same spectrograph configuration. The exposure times were 3×150 s for both targets. We measured a signal-to-noise S/N ~ 300 for each of the binary components, with a spectral coverage between 3870–6900 Å. The asteroid Ganymede was also observed with the same spectrograph set-up achieving a slightly higher S/N, to acquire the solar spectrum useful for reference in our (initial) differential analysis. We note however that the final differential study with the highest abundance precision is between ζ^1 Ret and ζ^2 Ret because of their high degree of similarity. The data were reduced with the HARPS pipeline and combined using the software package IRAF⁴.

3. Stellar parameters and chemical abundance analysis

We derived the fundamental parameters (T_{eff} , $\log g$, [Fe/H], v_{turb}) of ζ^1 Ret and ζ^2 Ret following the same procedure detailed in our previous work (Saffe et al. 2015). We started by measuring the equivalent widths (EW) of Fe I and Fe II lines in the spectra of our program stars using the IRAF task *splot*, and then continued with other chemical species. The lines list and relevant laboratory data (such as excitation potential and oscillator strengths) were taken from Liu et al. (2014), Meléndez et al. (2014), and then extended with data from Bedell et al. (2014), who carefully selected lines for a high-precision abundance determination. This data, including the measured EWs, are presented in Table 1. Then, we imposed excitation and ionization balance of Fe I and Fe II lines, using the differential version of the program FUNDPAR (Saffe 2011), together with the 2014 version of the MOOG code (Sneden 1973) and ATLAS9 model atmospheres (Kurucz 1993).

Stellar parameters of ζ^1 Ret and ζ^2 Ret were differentially determined using the Sun as standard in an initial approach, and then we recalculated the parameters of ζ^1 Ret using ζ^2 Ret as reference. First, we determined absolute abundances for the Sun using 5777 K for T_{eff} , 4.44 dex for $\log g$ and an initial v_{turb} of 1.0 km/s. Then, we estimated v_{turb} for the Sun with the usual method of requiring zero slope in the absolute abundances of Fe I lines versus EW_r , and obtained a final v_{turb} of 0.91 km/s. We note however that the exact values are not crucial for our strictly differential study (see e.g. Bedell et al. 2014; Saffe et al. 2015).

The next step was the determination of stellar parameters of ζ^1 Ret and ζ^2 Ret using the Sun as standard, i.e. (ζ^1 Ret - Sun) and (ζ^2 Ret - Sun). For ζ^1 Ret the resulting stellar parameters were $T_{eff} = 5710 \pm 29$ K, $\log g = 4.53 \pm 0.05$ dex, [Fe/H] = -0.195 ± 0.005 dex, and $v_{turb} = 0.80 \pm 0.27$ km/s. For ζ^2 Ret, we obtained $T_{eff} = 5854 \pm 28$ K, $\log g = 4.54 \pm 0.04$ dex, [Fe/H] = -0.215 ± 0.004 dex, and $v_{turb} = 0.95 \pm 0.09$ km/s. In the Table 2 we present the differential parameters ΔT_{eff} , $\Delta \log g$, $\Delta(\text{Fe/H})$ and Δv_{turb} derived between the star and their corresponding reference. The errors in the stellar parameters were derived following the procedure detailed in Saffe et al. (2015), which takes into account the individual and the mutual covariance terms of the

Table 2. Differential parameters ΔT_{eff} , $\Delta \log g$, $\Delta(\text{Fe/H})$ and Δv_{turb} derived between the star and their corresponding reference.

(Star - Reference)	ΔT_{eff} [K]	$\Delta \log g$ [dex]	$\Delta(\text{Fe/H})$ [dex]	Δv_{turb} [km/s]
(ζ^1 Ret - Sun)	-67 ± 29	$+0.09 \pm 0.05$	-0.195 ± 0.005	-0.11 ± 0.27
(ζ^2 Ret - Sun)	$+77 \pm 28$	$+0.10 \pm 0.04$	-0.215 ± 0.004	$+0.04 \pm 0.09$
(ζ^1 Ret - ζ^2 Ret)	-144 ± 22	-0.01 ± 0.03	$+0.020 \pm 0.003$	-0.15 ± 0.07

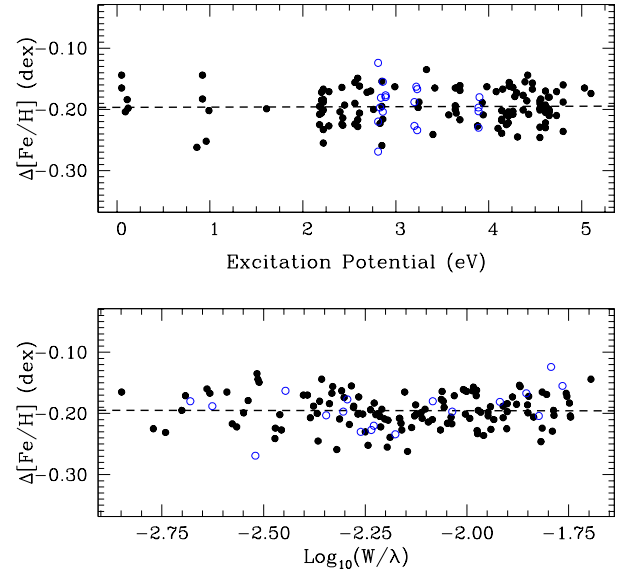


Fig. 1. Differential abundance vs excitation potential (upper panel) and differential abundance vs reduced EW (lower panel), for ζ^1 Ret relative to the Sun. Filled and empty points correspond to Fe I and Fe II, respectively. The dashed line is a linear fit to the abundance values.

error propagation. The star ζ^1 Ret resulted with a slightly higher metallicity than ζ^2 Ret by ~ 0.02 dex. Figures 1 and 2 show abundance vs excitation potential and abundance vs EW_r , for both stars. Filled and empty points correspond to Fe I and Fe II, while the dashed lines are linear fits to the differential abundance values.

Then, the parameters of ζ^1 Ret were recalculated but using ζ^2 Ret as reference instead of the Sun, i.e. (ζ^1 Ret - ζ^2 Ret). Figure 3 shows abundance vs excitation potential and abundance vs EW_r , using similar symbols to those used in Figures 1 and 2. The resulting stellar parameters for ζ^1 Ret are the same to that obtained when we used the Sun as a reference, but with lower dispersions: $T_{eff} = 5710 \pm 22$ K, $\log g = 4.53 \pm 0.03$ dex, [Fe/H] = -0.195 ± 0.003 dex, and $v_{turb} = 0.80 \pm 0.07$ km/s. The differential parameters ΔT_{eff} , $\Delta \log g$, $\Delta(\text{Fe/H})$ and Δv_{turb} derived between ζ^1 Ret and ζ^2 Ret are also presented in the Table 2. Again, we found that the metallicity of ζ^1 Ret is slightly higher than ζ^2 Ret by ~ 0.02 dex.

Once the stellar parameters of the binary components were determined using iron lines, we computed abundances for all remaining chemical elements. The hyperfine structure splitting (HFS) was considered for V I, Mn I, Co I, Cu I, and Ba II, using the HFS constants of Kurucz & Bell (1995) and performing spectral synthesis for these species. We derived the O I abundances by using spectral synthesis with the line 6300.304 Å⁵. (the O I triplet is out of the HARPS wavelength range), which is basically free of NLTE effects (Takeda 2003). Direct interpo-

³ <https://www.eso.org/sci/facilities/lasilla/instruments/harps/tools/archive.html>

⁴ IRAF is distributed by the National Optical Astronomical Observatories, which is operated by the Association of Universities for Research in Astronomy, Inc. under a cooperative agreement with the National Science Foundation.

⁵ This line is blended with Ni I 6300.336 Å.

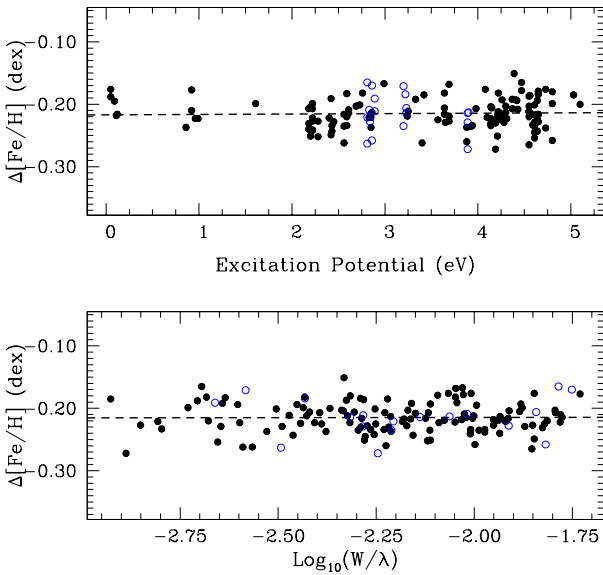


Fig. 2. Differential abundance vs excitation potential (upper panel) and differential abundance vs reduced EW (lower panel), for ζ^2 Ret relative to the Sun. Filled and empty points correspond to Fe I and Fe II, respectively. The dashed line is a linear fit to the abundance values.

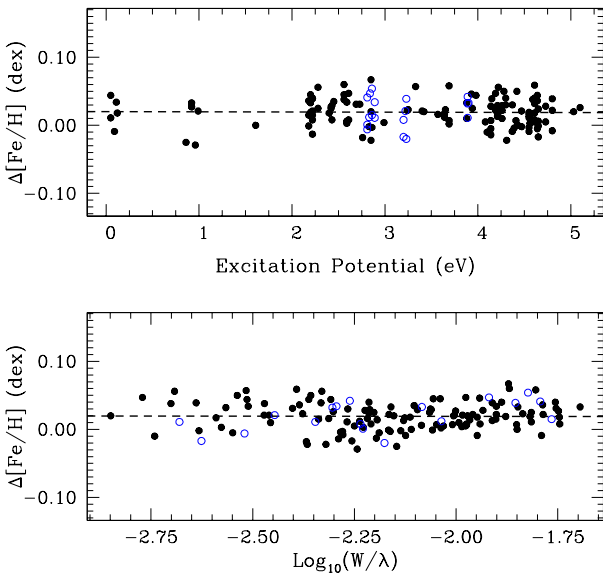


Fig. 3. Differential abundance vs excitation potential (upper panel) and differential abundance vs reduced EW (lower panel), for ζ^1 Ret relative to ζ^2 Ret. Filled and empty points correspond to Fe I and Fe II, respectively. The dashed line is a linear fit to the data.

lation in the tables of Amarsi et al. (2015) results also in a null NLTE correction for this O I line. We also applied NLTE corrections to Ba II (-0.10 dex) and Cu I (+0.04 dex) in the same amount for both stars, interpolating in data of Korotin et al. (2011) and Yan et al. (2015).

In Table 3 we present the final differential abundances $[X/Fe]^6$ of ζ^1 Ret and ζ^2 Ret relative to the Sun, and the differential abundances of ζ^1 Ret using ζ^2 Ret as the reference star. We present both the observational errors σ_{obs} (estimated as

Table 4. Derived slopes (abundance vs temperature condensation T_c), their dispersion and probability of the slope "being by chance" (see text for details).

(Star - Reference)	Slope $\pm \sigma$	Prob.
	[10^{-5} dex/K]	
$(\zeta^1 \text{ Ret} - \text{Sun})$	$+3.31 \pm 2.23$	0.48
$(\zeta^2 \text{ Ret} - \text{Sun})$	-2.57 ± 1.99	0.52
$(\zeta^1 \text{ Ret} - \zeta^2 \text{ Ret})$	$+6.27 \pm 1.55$	0.27
$(\zeta^1 \text{ Ret} - \zeta^2 \text{ Ret})_{Ref}$	$+3.85 \pm 1.02$	0.29

$\sigma / \sqrt{n-1}$, where σ is the standard deviation of the different lines) and systematic errors due to uncertainties in the stellar parameters σ_{par} (by adding quadratically the abundance variation when modifying the stellar parameters by their uncertainties), as well as the total error σ_{TOT} obtained by quadratically adding σ_{obs} , σ_{par} and the error in [Fe/H].

4. Results and discussion

The differential abundances of ζ^1 Ret and ζ^2 Ret relative to the Sun are presented in Figures 4 and 5, with condensation temperatures taken from the 50% T_c values derived by Lodders (2003). We corrected by GCE effects when comparing (star-Sun) following the same procedure of Saffe et al. (2015) by adopting the GCE fitting trends of González Hernández et al. (2013). However, this correction is discarded when comparing mutually the components of the binary system (ζ^1 Ret - ζ^2 Ret), due to their common natal environment. Filled points in Figs. 4 and 5 correspond to the differential abundances for the stars ζ^1 Ret and ζ^2 Ret relative to the Sun. The continuous line correspond to the solar-twins trend of M09 (vertically shifted for comparison), while the dashed line in Figs. 4 and 5 is a linear fit to the abundance values. We also present in the Table 4 the derived slopes with their dispersions. In order to provide another estimation of the significance of the slopes, we performed 100000 series of simulated random abundances and errors, following a similar method to MA15. Then, assuming that the distribution of the simulated slopes follows a Gaussian distribution, we compute the probability of the original slope "being by chance". This value is also presented in the last column of Table 4.

We note that the general trend of ζ^1 Ret presents a slightly higher slope than the Sun, while ζ^2 Ret presents a slightly lower slope than the Sun. This would correspond, for instance, to an slight lack of refractories ($T_c > 900$ K) respect to volatiles ($T_c < 900$ K) when comparing ζ^2 Ret with the Sun. However, the general trends should be taken with caution due to the relatively high dispersion of points (most elements spread between -0.20 dex and +0.20 dex). These dispersions are greatly diminished by comparing mutually ζ^1 Ret and ζ^2 Ret, which present the advantage of the strong similarity between them, together with the independence of GCE and evolutionary effects. Also, as we see in Table 4, the slopes of the stars relative to the Sun are derived within $\sim 1.5\sigma$, while for the case $(\zeta^1 \text{ Ret} - \zeta^2 \text{ Ret})$ the slope values are within $\sim 4\sigma$ i.e. the significance of the slope increases significantly. The Table 4 also includes the case of considering only the refractory elements between ζ^1 Ret and ζ^2 Ret, showed as $(\zeta^1 \text{ Ret} - \zeta^2 \text{ Ret})_{Ref}$. The probability of the slopes "being by chance" are relatively high when the Sun is used as reference ($\sim 50\%$), however these values are diminished ($\sim 28\%$) in the mutual comparison (ζ^1 Ret - ζ^2 Ret), and are similar to those derived by MA15 (see e.g their Table 9).

⁶ We used the standard notation $[X/Fe] = [X/H] - [\text{Fe}/H]$

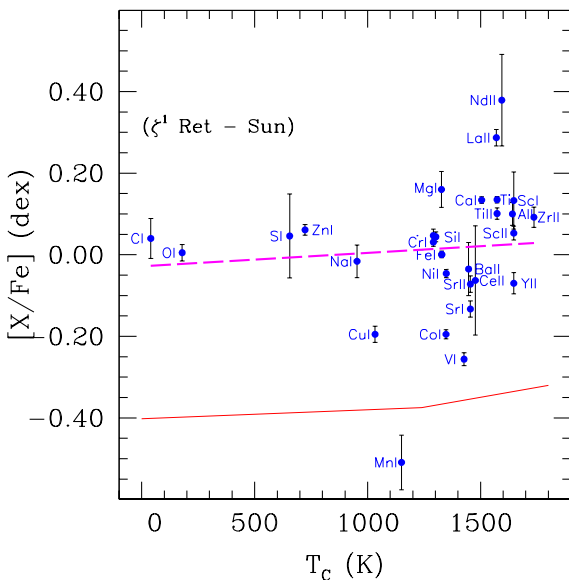


Fig. 4. Differential abundances (ζ^1 Ret - Sun) vs condensation temperature T_c . The dashed line is a linear fit to the differential abundance values, while the continuous line shows the solar-twins trend of Meléndez et al. (2009).

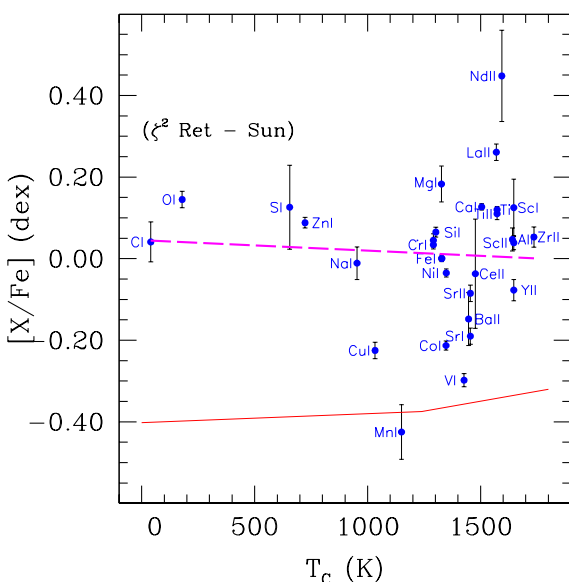


Fig. 5. Differential abundances (ζ^2 Ret - Sun) vs condensation temperature T_c . The dashed line is a linear fit to the differential abundance values, while the continuous line shows the solar-twins trend of Meléndez et al. (2009).

The abundances of Mn I and Nd II seem to deviate from the general trends for both stars (see Figs. 4 and 5). We derived the abundances of Mn I including the hyperfine structure splitting (HFS) using the constants of Kurucz & Bell (1995) in the spectral synthesis. We do not detect an HFS abundance difference between the Mn I line 4502.21 Å and other Mn I lines, as reported by MA15. For the Sun, Bergemann & Gehren (2007) estimated maximum NLTE corrections of +0.1 dex for Mn, however even with such maximum correction the Mn abundance still results relatively low. Given the similar parameters of our stars with the Sun, we consider that the NLTE effects could also play a role in

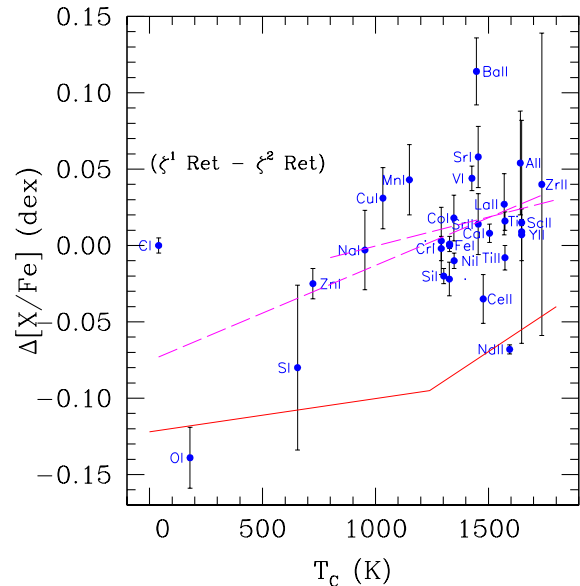


Fig. 6. Differential abundances (ζ^1 Ret - ζ^2 Ret) vs condensation temperature T_c . The long-dashed lines are linear fits to all species and to the refractory species. The solar-twins trend of Meléndez et al. (2009) is shown with a continuous line.

ζ^1 Ret and ζ^2 Ret. The abundance of Nd II was derived using the Equivalent Widths of two lines (4021.33 Å and 4446.38 Å). We have no evidence of an obvious blend at these lines, however it is difficult to discard this possibility. Other Nd II lines such as 4059.95 Å or 5234.19 Å are very weak. Mashonkina et al. (2005) studied NLTE effects of Nd II but in stars with higher temperatures (>7500 K). Then, in order to derive representative trends we excluded Mn I and Nd II from the linear fits.

The differential abundances of ζ^1 Ret using ζ^2 Ret as reference are presented in Fig. 6. In our calculation, this plot corresponds to the abundance values derived with the highest possible precision. The continuous line in this Figure presents the solar-twins trend of M09 (vertically shifted), while the long-dashed lines are linear fits to all elements as well as the refractory elements. The differential abundances of the refractories (average of +0.016 dex) are higher than the volatiles (average of -0.061 dex), with a general slope of $6.27 \pm 1.55 \cdot 10^{-5}$ dex/K, as we see in the Fig. 6. Although the general trend seems to be driven by O I (which present a relatively low abundance value), when excluding O I the slope results $3.96 \pm 1.05 \cdot 10^{-5}$ dex/K i.e. a general trend even closer to the refractory trend. The refractory elements (alone) also show a trend with T_c , with a slope of $3.85 \pm 1.02 \cdot 10^{-5}$ dex/K. For comparison, the slope of refractories between the components of the binary system 16 Cyg resulted $1.88 \cdot 10^{-5}$ dex/K and clearly showing a higher abundance in refractory than volatile elements (Tucci Maia et al. 2014). We caution, however, that there is still no total consensus on the possible chemical differences between the components of 16 Cyg (e.g. Takeda 2005; Schuler et al. 2011b; Tucci Maia et al. 2014). Then, the higher value of the refractory elements compared to volatile elements, together with the positive slope in the trend of refractory elements with T_c , point toward a lack of refractory elements in ζ^2 Ret relative to ζ^1 Ret.

Detailed abundance studies performed on binary systems with similar components (where at least one component hosts a planet) showed different results. Some binary systems such as HAT-P-1 and HD 80606 does not seem to present significant T_c

trends between their components (Liu et al. 2014; Saffe et al. 2015). On the other hand, the binary systems XO-2 and HD 20781 seem to present a relative T_c trend (Biazzo et al. 2015; Mack et al. 2014), although they are particular cases, given that both components of the system host a planet. Also, possible metallicity differences of wide binary stars and multiple systems have been studied in the literature. Most of the cases present almost no metallicity differences, similar to the case of the triple system HD 132563 (Desidera et al. 2011). However, $\sim 17\%$ of the wide binaries do present slight metallicity differences between their components (Desidera et al. 2004, 2006). The origin of these slight differences is not totally clear, and a possible explanation lies the planet formation process (e.g. Desidera et al. 2004, 2006).

Following the interpretation of M09 and R10, the lack of refractory elements in ζ^2 Ret compared to ζ^1 Ret could be identified with the signature of the planet formation process. Because no planets are detected around the stars of this binary system, the refractory elements depleted in ζ^2 Ret are possibly locked-up in rocky bodies (e.g. planetesimals and/or asteroids) whose collisions could produce the bright debris disk observed in this object. In fact, the slightly lower metallicity of ζ^2 Ret compared to their companion (by ~ 0.02 dex) is also compatible with this scenario. Probably, the relatively low metallicity of both stars prevented the formation of giant planets in this binary system. However the presence of circumstellar material around ζ^2 Ret (the debris disk) has been confirmed, as we mentioned previously. The fact that the conditions required to form a debris-disk are more easily met than the conditions to form gas-giant planets, is in agreement with the core-accretion model of planet formation (e.g. Pollack et al. 1996; Mordasini et al. 2012).

The rocky mass of depleted material in ζ^2 Ret was estimated following Chambers (2010), in order to reproduce the trend of the refractory elements of Fig. 6. Using a convection zone similar to the Sun ($M_{cz} = 0.023 M_\odot$) we obtain $M_{rock} \sim 3 M_\oplus$. However, at the time of the planet formation process M_{cz} could be greater than this value. For instance, adopting $M_{cz} = 0.050 M_\odot$ we derive $M_{rock} \sim 7 M_\oplus$. Then, $M_{rock} \sim 3 M_\oplus$ should be considered as a lower limit. On the other hand, there is no direct estimation for the debris disk mass of ζ^2 Ret (see e.g. Eiroa et al. 2010; Faramaz et al. 2014). The most precise estimates debris disk masses comes from sub-mm observations (see e.g. Wyatt 2008). Krivov et al. (2008) modeled 5 solar-type debris-disk stars and fitted the far-IR emission using disk masses in the range $3\text{-}50 M_\oplus$ and radii between 100-200 AU. The mass range and radii are compatible with the mass derived from Chambers (2010) and the observed location of the disk around ζ^2 Ret ($R \sim 100$ AU, Eiroa et al. 2010). However, Krivov et al. (2008) caution that the mass and location of the debris disk depend significantly on the collisional model and grain properties adopted.

5. Conclusions

We performed a high-precision differential abundance determination in both components of the remarkable binary system ζ^1 Ret - ζ^2 Ret, in order to detect a possible T_c trend. Both stars present very similar stellar parameters, which greatly diminishes the errors in the abundance determination, GCE or evolutionary effects. The star ζ^2 Ret hosts a debris disk, while there is no debris disk detected (nor a planet) around ζ^1 Ret. First, we derived stellar parameters and differential abundances of both stars using the Sun as the reference star and then for ζ^1 Ret using ζ^2 Ret as reference. Our calculation included NLTE corrections for Ba II and Cu I as well as GCE corrections for all chemical species,

where the Sun was used as reference. We compared the possible temperature condensation T_c trends of the stars with the solar-twins trend of Meléndez et al. (2009).

In comparing the stars to each other, ζ^1 Ret resulted slightly more metal rich than ζ^2 Ret by ~ 0.02 dex. Also, the differential abundances of the refractories resulted higher than the volatiles, and the general trend of the refractory elements with T_c showed a positive slope. These facts together point toward a lack of refractory elements in ζ^2 Ret relative to ζ^1 Ret, similar to the case of the binary system 16 Cyg (Tucci Maia et al. 2014). We caution, however, that there is still no total consensus on the possible chemical differences between the components of 16 Cyg (e.g. Takeda 2005; Schuler et al. 2011b; Tucci Maia et al. 2014). We note that the statistical result of Maldonado et al. (2015) does not exclude possible T_c trends in particular stars such as the ζ Ret system. Then, following the interpretation of M09 and R10, we propose an scenario in which the refractory elements depleted in ζ^2 Ret are possibly locked-up in the rocky material that orbits this star and produce the debris disk observed around this object. We estimated a lower limit of $M_{rock} \sim 3 M_\oplus$ for the rocky mass of depleted material according to Chambers (2010), which is compatible with a rough estimation of $3\text{-}50 M_\oplus$ of a debris disk mass around a solar-type star (Krivov et al. 2008). We strongly encourage high-precision abundance studies in binary systems with similar components, which is a crucial tool for helping to detect the possible chemical pattern of the planet formation process.

Acknowledgements. The authors thank Drs. R. Kurucz and C. Sneden for making their codes available to us. We also thank the anonymous referee for constructive comments that improved the paper.

References

- Adibekyan, V., González Hernández, J., Delgado-Mena, E., et al., 2014, A&A 564, L15
- Allende Prieto, C., Barklem, P., Lambert, D., Cunha, K., 2004, A&A 420, 183
- Amarsi, A., Asplund, M., Collet, R., Leenaarts, J., 2015, MNRAS 455, 3735
- Aumann, H. H., Beichman, C. A., Gillett, F. C., et al. 1984, ApJ, 278, 23
- Bedell, M., Meléndez, J., Bean, J., et al., 2014, AJ 795, 23
- Beichman, C., Bryden, G., Rieke, G., et al., 2005, AJ 622, 1160
- Beichman, C. A., Bryden, G., Stapelfeldt, K. R., et al. 2006a, ApJ, 652, 1674
- Bensby, T., Feltzing, S., Oey, M., 2014, A&A 562, A71
- Bergemann, M., Gehren, T., 2007, A&A 473, 291
- Biazzo, K., Gratton, R., Desidera, S., et al., 2015, A&A 583, A135
- Bryden, G., Beichman, C. A., Trilling, D. E., et al. 2006, ApJ, 636, 1098
- Chambers, J., 2010, ApJ 724, 92
- Currie, T., Lisse, C., Kuchner, M., et al., 2015, ApJL 807, L7
- Desidera, S., Gratton, R. G., Scuderi, S., Claudi, R. U., Cosentino, R., Barbieri, M., Bonanno, G., Carretta, E., Endl, M., Lucatello, S., Martínez Fiorenzano, A. F., Marzari, F., 2004, A&A 420, 683
- Desidera, S., Gratton, R. G., Lucatello, S., Claudi, R. U., 2006, A&A 454, 581
- Desidera, S., Carolo, E., Gratton, R., et al., 2011, A&A 533, A90
- Eiroa, C., Fedele, D., Maldonado, J., et al., 2010, A&A 518, L131
- Eiroa, C., Marshall, J., Mora, A., et al., 2013, A&A 555, 11
- Faramaz, V., Beust, H., Thébault, P., et al., 2014, A&A 563, A72
- Gonzalez, G., Carlson, M., Tobin, W., 2010, MNRAS 407, 314
- Gonzalez, G., 2011, MNRASL 416, L80
- González Hernández, J., Delgado-Mena, E., Sousa, S., et al., 2013, A&A 552, A6
- Habing, H. J., Dominik, C., Jourdain de Muizon, M., et al. 2001, A&A, 365, 545
- Korotin, S., Mishenina, T., Gorbaneva, T., Soubiran, C., 2011, MNRAS 415, 2093
- Krist, J., Ardila, D., Goliowski, D., et al., 2005, AJ 129, 1008
- Krivov, A., Müller, S., Löhne, T., Mutschke, H., 2008, AJ 687, 608
- Kurucz, R. L. 1993, ATLAS9 Stellar Atmosphere Programs and 2 km/s grid, Kurucz CD-ROM No. 13, Smithsonian Astrophysical Observatory, Cambridge, MA.
- Kurucz, R., Bell, B., 1995, *Atomic Line Data*, Kurucz CD-ROM No. 23, Smithsonian Astrophysical Observatory, Cambridge, MA.

- Liu, F., Asplund, M., Ramírez, I., Yong, D., Meléndez, J., 2014, MNRASL 442, L51
- Lodders, K., 2003, AJ 591, 1220
- Löhne, T., Eiroa, C., Augereau, J.-C., et al., 2012, AN 333, 441
- Mack, C., Schuler, S., Stassun, K., Norris, J., 2014, ApJ 787, 98
- Maldonado, J., Eiroa, C., Villaver, E., et al., 2012, A&A 541, A40
- Maldonado, J., Eiroa, C., Villaver, E., Montesinos, B., Mora, A., 2015, A&A 579, A20
- Mannings, V., Barlow, M. J. 1998, ApJ, 497, 330
- Mashonkina, L., Ryabchikova, T., Ryabtsev, A., 2005, A&A 441, 309
- Mason, B., Wycoff, G., Hartkopf, W., Douglass, G., Worley, C. E., 2001, AJ, 122, 3466
- Matthews, B., Sibthorpe, B., Kennedy, G., et al., 2010, A&A 518, L135
- Matthews, B., Krivov, A., Wyatt, M., Bryden, G., Eiroa, C., 2014, Protostars and Planets VI, Henrik Beuther, Ralf S. Klessen, Cornelis P. Dullemond, and Thomas Henning (eds.), University of Arizona Press, Tucson, 914 pp., p. 521-544
- Mayor, M., Pepe, F., Queloz, D., et al., 2003, The Messenger 114, 20
- Meléndez, J., Asplund, M., Gustafsson, B., Yong, D., 2009, AJ 704, L66
- Meléndez, J., Ramírez, I., Karakas, A., Yong, D., Monroe, T., et al. 2014, AJ 791, 14
- Mordasini, C., Alibert, Y., Benz, W., et al., 2012, A&A 541, A97
- Moro-Martín, A. 2013, in Dusty Planetary Systems, ed. T. D. Oswalt, L. M. French, & P. Kalas (Hamburg: Springer Verlag), 431
- Phillips, N., Graves, J., Dent, W., et al., 2010, MNRAS 403, 1089
- Pollack, J. B., Hubickyj, O., Bodenheimer, P., et al., 1996, Icarus, 124, 62
- Ramírez, I., Asplund, M., Baumann, P., Meléndez, J., Bensby, T., 2010, A&A 521, A33
- Rieke, G., Su, K., Stansberry, J., et al., 2005, AJ 620, 1010
- Rodriguez, D., Zuckerman, B., 2012, AJ 745, 147
- Rodriguez, D., Duchene, G., Tom, H., et al., 2015, MNRAS 449, 3160
- Saffe, C., 2011, RMxAA 47, 3
- Saffe, C., Flores, M., Buccino, A., 2015, A&A 582, A17
- Schuler, S., Flateau, D., Cunha, K., et al., 2011, AJ 732, 55
- Schuler, S., Cunha, K., Smith, V., et al., 2011, ApJL 737, L32
- Shaya, E., Olling, R., 2011, ApJS 192, 2
- Smith, B., Terriere, R., 1984, Science 226, 1421
- Sneden, C., ApJ 184, 839
- Soumer, R., Perrin, M., Pueyo, L., et al. 2014, ApJL 786, L23
- Sousa, S., Santos, N., Mayor, M., et al., 2008, A&A 487, 373
- Su, K. Y., Rieke, G., Stansberry, J., et al., 2006, AJ 653, 675
- Takeda, Y., 2003, A&A 402, 343
- Takeda, Y., 2005, PASJ 57, 83
- Trilling, D., Stansberry, J., Stapelfeldt, K., et al., 2007, ApJ 658, 1289
- Trilling, D., Bryden, G., Beichman, C., et al., 2008, AJ 674, 1086
- Tucci Maia, M., Meléndez, J., Ramírez, I., 2014, ApJL 790, L25
- Vandenbussche, B., Sibthorpe, B., Acke, B., et al. 2010, A&A 518, L133
- Wittenmyer, R., O'Toole, S., Jones, H., et al., 2010, AJ 722, 1854
- Wyatt, M., 2008, Annu. Rev. Astron. Astrophys. 46, 339
- Yan, H., Shi, J., Zhao, G., 2015, AJ 802, 36

Table 1. Line list used in this work. The columns present the element, wavelength λ , excitation potential (EP), log gf , equivalent widths of ζ^1 Ret, ζ^2 Ret, and Sun (EW_1 , EW_2 , and EW_{Sun}). The abundances of lines without EWs were measured using synthetic spectra.

Element	λ [Å]	EP [eV]	log gf [dex]	EW_1 [mÅ]	EW_2 [mÅ]	EW_{Sun} [mÅ]
	6.00	5052.167	7.680	-1.240	23.3	25.4
	6.00	6587.610	8.540	-1.050	8.3	9.6
	8.00	6300.304	0.000	-9.820		
	11.00	4751.822	2.100	-2.080	9.4	7.7
	11.00	5148.838	2.100	-2.040	9.0	6.7
	11.00	6154.225	2.100	-1.550	24.3	23.0
	11.00	6160.747	2.100	-1.250	42.8	36.9
	12.00	4571.095	0.000	-5.620	102.8	97.2
	12.00	4730.040	4.340	-2.390	58.2	54.0
	12.00	5711.088	4.340	-1.730	102.2	94.8
	12.00	6318.717	5.110	-1.950	32.7	28.7
	12.00	6319.236	5.110	-2.160	29.8	26.3
	13.00	5557.070	3.140	-2.210	9.3	6.1
	13.00	6696.018	3.140	-1.480	30.9	25.9
	13.00	6698.667	3.140	-1.780	15.7	12.1
	14.00	5488.983	5.610	-1.690	11.0	11.9
	14.00	5517.540	5.080	-2.500	9.6	8.1
	14.00	5645.611	4.930	-2.040	27.3	25.8
	14.00	5665.554	4.920	-1.940	31.9	28.9
	14.00	5684.484	4.950	-1.550	49.7	46.8
	14.00	5690.425	4.930	-1.770	38.5	36.5
	14.00	5701.104	4.930	-1.950	30.4	28.7
	14.00	5753.640	5.620	-1.330	36.0	34.8
	14.00	5772.145	5.082	-1.653	42.2	41.7
	14.00	5793.073	4.930	-1.960	35.0	31.8
	14.00	5948.540	5.080	-1.208	80.0	77.8
	14.00	6125.021	5.610	-1.500	23.1	21.5
	14.00	6142.490	5.620	-1.540	26.9	25.7
	14.00	6145.015	5.620	-1.410	27.4	25.9
	14.00	6195.460	5.870	-1.666	10.1	9.6
	14.00	6237.330	5.610	-1.116	50.4	47.0
	14.00	6243.823	5.620	-1.270	34.7	33.5
	14.00	6244.476	5.620	-1.320	34.4	33.9
	14.00	6527.210	5.870	-1.230	33.6	32.0
	14.00	6721.848	5.860	-1.120	30.8	30.7
	14.00	6741.630	5.980	-1.650	9.3	9.4
	16.00	4695.443	6.530	-1.830	4.9	5.7
	16.00	6052.656	7.870	-0.400	4.7	6.8
	20.00	4512.268	2.530	-1.900	18.4	15.6
	20.00	5260.387	2.520	-1.720	27.2	23.0
	20.00	5261.710	2.520	-0.680	95.6	89.6
	20.00	5512.980	2.930	-0.460	81.4	73.4
	20.00	5581.965	2.520	-0.560	91.6	84.7
	20.00	5590.114	2.520	-0.570	88.5	79.7
	20.00	5867.562	2.930	-1.570	18.5	13.7
	20.00	6156.020	2.520	-2.497	6.4	5.1
	20.00	6161.297	2.520	-1.270	55.1	49.2
	20.00	6166.439	2.520	-1.140	62.0	55.5
	20.00	6169.042	2.520	-0.800	88.4	79.7
	20.00	6169.550	2.520	-0.580	110.3	98.7
	20.00	6455.598	2.520	-1.340	50.6	43.0
	20.00	6471.662	2.530	-0.690	85.7	80.3
	20.00	6499.650	2.520	-0.820	80.3	73.8
	20.00	6572.800	0.000	-4.280	27.4	19.9
	21.00	4743.821	1.450	0.350	7.5	4.8
	21.00	5671.821	1.450	0.550	10.7	8.6
	21.10	5526.820	1.770	0.140	68.8	69.0
						76.2

Table 1. Continued.

Element	λ [Å]	EP [eV]	$\log gf$ [dex]	EW_1 [mÅ]	EW_2 [mÅ]	EW_{Sun} [mÅ]
21.10	5657.870	1.510	-0.300	59.8	59.8	65.7
21.10	5667.140	1.500	-1.020	25.6	24.5	34.6
21.10	6245.630	1.510	-1.030	28.2	26.8	36.5
21.10	6604.578	1.360	-1.150	28.3	26.9	37.1
22.00	4465.802	1.740	-0.160	35.0	27.2	38.6
22.00	4512.733	0.840	-0.420	64.3	55.7	66.0
22.00	4555.485	0.850	-0.490	59.8	54.4	63.6
22.00	4617.280	1.750	0.450	60.9	53.4	62.4
22.00	4623.100	1.740	0.170	53.8	46.0	60.9
22.00	4645.190	1.730	-0.670	20.4	15.2	20.9
22.00	4656.470	0.000	-1.310	67.7	58.8	68.7
22.00	4722.610	1.050	-1.430	16.1	12.3	15.9
22.00	4758.120	2.250	0.430	39.4	33.0	43.0
22.00	4759.272	2.260	0.510	42.3	36.5	47.0
22.00	4778.258	2.240	-0.220	12.0	9.7	16.7
22.00	4820.410	1.500	-0.440	39.5	31.5	43.8
22.00	4840.880	0.900	-0.450	61.7	57.3	65.8
22.00	4913.616	1.870	0.160	48.5	39.9	49.7
22.00	4999.500	0.830	0.270	101.9	93.3	103.3
22.00	5022.871	0.830	-0.430	70.1	62.9	72.9
22.00	5024.850	0.820	-0.560	64.4	57.0	70.2
22.00	5039.960	0.020	-1.200	76.0	69.5	75.7
22.00	5071.490	1.460	-0.800	24.8	20.8	27.3
22.00	5113.448	1.440	-0.780	24.6	19.1	27.1
22.00	5147.479	0.000	-2.010	33.0	24.7	35.7
22.00	5219.700	0.020	-2.240	24.1	17.1	28.3
22.00	5295.774	1.070	-1.630	10.8	8.0	13.4
22.00	5471.200	1.440	-1.400	7.2	5.2	7.4
22.00	5490.150	1.460	-0.930	18.1	14.4	20.6
22.00	5689.459	2.300	-0.360	9.6	6.9	12.9
22.00	5739.464	2.250	-0.600	6.3	4.6	7.7
22.00	5866.452	1.070	-0.840	42.7	35.1	48.9
22.00	5965.840	1.880	-0.490	27.4	20.4	27.2
22.00	5978.550	1.870	-0.602	20.0	14.6	22.2
22.00	6064.630	1.050	-1.959	6.8	4.4	7.9
22.00	6091.174	2.270	-0.420	12.2	8.2	15.2
22.00	6126.217	1.070	-1.420	18.7	13.4	20.8
22.00	6258.104	1.440	-0.350	47.2	38.3	50.9
22.00	6261.101	1.430	-0.480	42.4	35.2	49.1
22.00	6312.234	1.460	-1.496	5.7	3.1	8.0
22.00	6599.104	0.900	-2.029	7.1	5.3	8.9
22.00	6743.130	0.899	-1.630	15.1	10.6	18.6
22.10	4470.857	1.160	-2.060	61.0	62.3	65.0
22.10	4544.028	1.240	-2.530	36.4	36.9	42.1
22.10	4609.265	1.180	-3.430	11.4	11.8	17.1
22.10	4657.212	1.240	-2.470	44.5	45.5	48.9
22.10	4779.985	2.048	-1.260	60.2	60.2	64.8
22.10	4798.532	1.080	-2.670	38.7	38.8	45.0
22.10	4865.611	1.120	-2.810	33.4	33.1	41.5
22.10	4874.014	3.100	-0.900	30.9	32.1	36.7
22.10	4911.193	3.120	-0.540	47.3	45.9	51.1
22.10	5381.015	1.570	-1.970	50.8	51.5	59.6
22.10	5418.767	1.580	-2.110	42.7	42.5	48.8
22.10	5490.690	1.570	-2.430	17.4	17.2	21.0
23.00	4875.442	0.040	-3.375			
23.00	4875.454	0.040	-2.260			
23.00	4875.461	0.040	-2.964			
23.00	4875.468	0.040	-1.420			
23.00	4875.471	0.040	-2.064			
23.00	4875.477	0.040	-2.742			

Table 1. Continued.

Element	λ [Å]	EP [eV]	$\log gf$ [dex]	EW_1 [mÅ]	EW_2 [mÅ]	EW_{Sun} [mÅ]
23.00	4875.483	0.040	-1.561			
23.00	4875.485	0.040	-2.010			
23.00	4875.491	0.040	-2.617			
23.00	4875.495	0.040	-1.725			
23.00	4875.497	0.040	-2.032			
23.00	4875.502	0.040	-2.566			
23.00	4875.505	0.040	-1.923			
23.00	4875.506	0.040	-2.123			
23.00	4875.509	0.040	-2.596			
23.00	4875.511	0.040	-2.178			
23.00	4875.511	0.040	-2.311			
23.00	4875.515	0.040	-2.566			
23.00	5703.555	1.050	-0.777			
23.00	5703.569	1.050	-0.993			
23.00	5703.569	1.050	-1.403			
23.00	5703.580	1.050	-1.242			
23.00	5703.580	1.050	-1.276			
23.00	5703.581	1.050	-2.268			
23.00	5703.589	1.050	-1.250			
23.00	5703.589	1.050	-1.715			
23.00	5703.590	1.050	-1.840			
23.00	5703.596	1.050	-1.414			
23.00	5703.596	1.050	-1.590			
23.00	5703.601	1.050	-1.414			
23.00	5727.008	1.080	-0.693			
23.00	5727.016	1.080	-1.701			
23.00	5727.022	1.080	-3.003			
23.00	5727.028	1.080	-0.798			
23.00	5727.035	1.080	-1.490			
23.00	5727.040	1.080	-2.605			
23.00	5727.045	1.080	-0.914			
23.00	5727.051	1.080	-1.417			
23.00	5727.056	1.080	-2.400			
23.00	5727.060	1.080	-1.043			
23.00	5727.065	1.080	-1.411			
23.00	5727.069	1.080	-2.303			
23.00	5727.072	1.080	-1.189			
23.00	5727.075	1.080	-1.458			
23.00	5727.078	1.080	-2.303			
23.00	5727.081	1.080	-1.359			
23.00	5727.084	1.080	-1.563			
23.00	5727.086	1.080	-2.458			
23.00	5727.087	1.080	-1.563			
23.00	5727.089	1.080	-1.759			
23.00	5727.091	1.080	-1.826			
23.00	5727.619	1.050	-1.456			
23.00	5727.619	1.050	-1.867			
23.00	5727.653	1.050	-1.753			
23.00	5727.653	1.050	-2.072			
23.00	5727.654	1.050	-1.867			
23.00	5727.681	1.050	-1.753			
23.00	5727.681	1.050	-1.878			
23.00	5727.681	1.050	-9.850			
23.00	5727.701	1.050	-2.054			
23.00	5727.702	1.050	-1.878			
23.00	6081.417	1.050	-1.814			
23.00	6081.418	1.050	-1.638			
23.00	6081.428	1.050	-1.638			
23.00	6081.428	1.050	-9.610			
23.00	6081.429	1.050	-1.513			

Table 1. Continued.

Element	λ [Å]	EP [eV]	$\log gf$ [dex]	EW_1 [mÅ]	EW_2 [mÅ]	EW_{Sun} [mÅ]
23.00	6081.443	1.050	-1.513			
23.00	6081.443	1.050	-1.832			
23.00	6081.444	1.050	-1.627			
23.00	6081.461	1.050	-1.627			
23.00	6081.462	1.050	-1.216			
23.00	6090.194	1.080	-0.700			
23.00	6090.201	1.080	-0.841			
23.00	6090.207	1.080	-1.005			
23.00	6090.208	1.080	-1.540			
23.00	6090.213	1.080	-1.203			
23.00	6090.213	1.080	-1.344			
23.00	6090.217	1.080	-1.290			
23.00	6090.217	1.080	-1.458			
23.00	6090.220	1.080	-2.655			
23.00	6090.221	1.080	-1.312			
23.00	6090.221	1.080	-1.846			
23.00	6090.223	1.080	-1.403			
23.00	6090.223	1.080	-2.244			
23.00	6090.225	1.080	-1.591			
23.00	6090.225	1.080	-2.022			
23.00	6090.226	1.080	-1.897			
23.00	6090.227	1.080	-1.846			
23.00	6090.227	1.080	-1.876			
23.00	6111.592	1.042	-1.701			
23.00	6111.632	1.042	-1.224			
23.00	6111.656	1.042	-1.224			
23.00	6111.696	1.042	-1.370			
23.00	6119.528	1.063	-0.360			
23.00	6199.149	0.286	-2.133			
23.00	6199.167	0.286	-2.238			
23.00	6199.182	0.286	-2.354			
23.00	6199.197	0.286	-2.483			
23.00	6199.201	0.286	-3.141			
23.00	6199.209	0.286	-2.629			
23.00	6199.212	0.286	-2.930			
23.00	6199.221	0.286	-2.799			
23.00	6199.221	0.286	-2.857			
23.00	6199.229	0.286	-2.851			
23.00	6199.230	0.286	-3.003			
23.00	6199.235	0.286	-2.898			
23.00	6199.238	0.286	-3.266			
23.00	6199.240	0.286	-3.003			
23.00	6199.243	0.286	-3.199			
23.00	6199.246	0.286	-4.443			
23.00	6199.251	0.286	-4.045			
23.00	6199.253	0.286	-3.840			
23.00	6199.253	0.286	-3.898			
23.00	6199.255	0.286	-3.743			
23.00	6199.255	0.286	-3.743			
23.00	6242.798	0.262	-2.054			
23.00	6242.798	0.262	-2.521			
23.00	6242.829	0.262	-2.375			
23.00	6242.837	0.262	-2.375			
23.00	6242.852	0.262	-2.396			
23.00	6242.868	0.262	-2.852			
23.00	6243.045	0.300	-2.712			
23.00	6243.060	0.300	-2.497			
23.00	6243.075	0.300	-2.420			
23.00	6243.087	0.300	-1.649			
23.00	6243.087	0.300	-2.409			

Table 1. Continued.

Element	λ [Å]	EP [eV]	$\log gf$ [dex]	EW_1 [mÅ]	EW_2 [mÅ]	EW_{Sum} [mÅ]
23.00	6243.097	0.300	-1.785			
23.00	6243.099	0.300	-2.452			
23.00	6243.106	0.300	-1.933			
23.00	6243.109	0.300	-2.555			
23.00	6243.114	0.300	-2.092			
23.00	6243.118	0.300	-2.776			
23.00	6243.120	0.300	-2.261			
23.00	6243.125	0.300	-2.428			
23.00	6243.129	0.300	-2.566			
23.00	6243.132	0.300	-2.580			
23.00	6243.140	0.300	-2.712			
23.00	6243.142	0.300	-2.776			
23.00	6243.143	0.300	-2.497			
23.00	6243.145	0.300	-2.555			
23.00	6243.146	0.300	-2.420			
23.00	6243.146	0.300	-2.452			
23.00	6243.147	0.300	-2.409			
23.00	6285.160	0.275	-1.540			
24.00	4511.900	3.090	-0.390	33.7	28.8	40.9
24.00	4545.945	0.940	-1.310	81.5	74.5	84.7
24.00	4626.180	0.970	-1.470	79.8	74.1	82.7
24.00	4700.599	2.710	-1.250	11.2	9.8	14.0
24.00	4708.017	3.170	0.090	50.9	45.9	55.5
24.00	4767.860	3.560	-0.600	12.7	11.1	17.4
24.00	4775.140	3.550	-1.020	5.2	4.9	7.5
24.00	4789.340	2.540	-0.350	57.6	51.2	64.8
24.00	4801.047	3.120	-0.130	42.7	39.1	49.0
24.00	4936.335	3.110	-0.250	36.6	32.4	43.9
24.00	5214.140	3.370	-0.740	13.4	11.6	16.7
24.00	5238.964	2.710	-1.270	12.1	10.7	15.8
24.00	5247.566	0.960	-1.590	76.6	67.7	81.5
24.00	5272.007	3.450	-0.420	18.7	15.1	21.5
24.00	5287.200	3.440	-0.870	7.9	5.8	10.8
24.00	5296.691	0.980	-1.360	89.8	80.4	94.2
24.00	5300.744	0.980	-2.130	49.5	43.9	58.3
24.00	5345.801	1.000	-0.950	110.6	99.1	113.5
24.00	5348.312	1.000	-1.210	93.7	85.0	98.3
24.00	5628.621	3.420	-0.760	11.2	7.7	13.6
24.00	5783.080	3.320	-0.430	23.1	19.6	29.8
24.00	5783.870	3.320	-0.290	33.5	28.1	45.3
24.00	5787.930	3.322	-0.080	36.0	32.9	46.1
24.00	6330.100	0.941	-2.900	19.4	15.0	26.5
24.00	6661.080	4.190	-0.190	7.3	6.2	13.0
24.00	6882.477	3.438	-0.375	24.8	18.6	31.9
24.00	6882.997	3.438	-0.420	26.9	23.9	29.2
24.10	4588.199	4.070	-0.590	63.9	65.2	69.6
24.10	4592.049	4.070	-1.250	41.0	41.9	47.7
24.10	4616.628	4.070	-1.210	38.7	40.4	47.2
24.10	5237.328	4.070	-1.090	44.8	47.8	52.8
24.10	5246.767	3.710	-2.440	11.6	10.2	14.0
24.10	5502.067	4.170	-2.050	12.0	14.1	16.0
25.00	4502.213	2.918	-0.340			
25.00	4738.905	3.769	-4.770			
25.00	4739.357	4.317	-2.970			
25.00	5399.499	3.850	-0.290			
25.00	5399.624	4.270	-4.490			
25.00	5399.653	4.270	-4.290			
25.00	6013.478	3.070	-0.869			
25.00	6013.499	3.070	-1.081			
25.00	6013.518	3.070	-1.354			

Table 1. Continued.

Element	λ [Å]	EP [eV]	$\log gf$ [dex]	EW_1 [mÅ]	EW_2 [mÅ]	EW_{Sun} [mÅ]
25.00	6013.527	3.070	-1.558			
25.00	6013.533	3.070	-1.764			
25.00	6013.538	3.070	-1.412			
25.00	6013.547	3.070	-1.433			
25.00	6013.553	3.070	-1.588			
25.00	6013.562	3.070	-1.910			
25.00	6013.566	3.070	-1.956			
25.00	6013.566	3.070	-2.513			
25.00	6013.567	3.070	-2.132			
25.00	6016.619	3.071	-1.541			
25.00	6016.646	3.071	-1.378			
25.00	6016.647	3.071	-0.763			
25.00	6016.667	3.071	-1.373			
25.00	6016.668	3.071	-1.026			
25.00	6016.685	3.071	-1.357			
25.00	6016.685	3.071	-1.475			
25.00	6016.696	3.071	-1.541			
25.00	6016.696	3.071	-1.804			
25.00	6016.699	3.071	-1.737			
25.00	6016.705	3.071	-2.503			
25.00	6016.707	3.071	-1.378			
25.00	6016.714	3.071	-1.373			
25.00	6016.714	3.071	-1.737			
25.00	6016.716	3.071	-1.475			
26.00	4365.900	2.990	-2.250	45.1	40.7	51.3
26.00	4389.250	0.050	-4.580	67.2	62.4	71.9
26.00	4602.000	1.610	-3.150	65.0	60.9	71.6
26.00	4635.850	2.850	-2.340	49.4	44.2	56.9
26.00	4745.800	3.650	-1.270	69.2	63.9	77.6
26.00	4749.950	4.560	-1.240	28.1	24.8	36.0
26.00	4779.440	3.420	-2.160	33.6	28.7	40.2
26.00	4788.760	3.240	-1.730	60.2	55.2	67.8
26.00	4799.410	3.640	-2.130	27.8	23.7	35.5
26.00	4808.150	3.250	-2.690	20.2	16.2	26.5
26.00	4994.130	0.920	-3.080	100.7	92.9	104.7
26.00	5044.211	2.850	-2.060	67.9	60.6	73.1
26.00	5054.642	3.640	-1.920	30.6	26.1	38.8
26.00	5090.770	4.260	-0.490	83.3	76.8	92.7
26.00	5109.650	4.300	-0.730	66.2	59.5	73.5
26.00	5127.359	0.920	-3.310	91.5	85.0	97.3
26.00	5127.679	0.050	-6.120	15.7	10.1	18.4
26.00	5141.740	2.420	-2.230	78.7	73.1	87.2
26.00	5145.090	2.200	-3.080	47.0	39.8	54.9
26.00	5187.910	4.140	-1.260	46.5	42.2	56.2
26.00	5198.711	2.220	-2.140	91.1	83.8	96.6
26.00	5225.525	0.110	-4.790	65.7	58.5	71.2
26.00	5243.770	4.260	-0.990	53.3	48.7	62.7
26.00	5247.050	0.090	-4.960	59.2	53.2	65.6
26.00	5250.208	0.120	-4.940	59.2	52.0	65.4
26.00	5288.520	3.690	-1.510	48.6	44.4	57.8
26.00	5295.312	4.420	-1.590	23.3	18.7	28.6
26.00	5373.709	4.470	-0.740	55.7	50.4	62.4
26.00	5379.574	3.690	-1.510	52.7	48.3	59.1
26.00	5386.334	4.150	-1.670	25.1	20.5	31.5
26.00	5389.480	4.410	-0.450	76.0	70.9	84.2
26.00	5409.130	4.370	-1.060	46.8	41.3	54.7
26.00	5441.340	4.310	-1.630	23.4	21.3	33.2
26.00	5464.280	4.140	-1.580	28.1	25.3	37.2
26.00	5466.987	3.570	-2.230	26.6	22.3	34.8
26.00	5472.710	4.210	-1.520	33.6	28.7	43.4

Table 1. Continued.

Element	λ [Å]	EP [eV]	$\log gf$ [dex]	EW_1 [mÅ]	EW_2 [mÅ]	EW_{Sun} [mÅ]
26.00	5491.830	4.190	-2.190	9.3	7.1	14.1
26.00	5522.446	4.210	-1.310	35.3	31.0	44.6
26.00	5543.940	4.220	-1.040	54.7	49.6	61.5
26.00	5546.506	4.370	-1.180	41.7	38.4	50.9
26.00	5554.890	4.550	-0.360	84.4	77.9	97.7
26.00	5560.211	4.430	-1.090	43.2	39.4	52.8
26.00	5577.020	5.030	-1.460	7.9	6.6	10.9
26.00	5618.633	4.210	-1.270	41.7	37.2	50.8
26.00	5636.696	3.640	-2.560	14.5	11.7	18.9
26.00	5638.262	4.220	-0.770	69.2	64.2	78.4
26.00	5649.987	5.100	-0.800	28.2	24.2	36.0
26.00	5651.469	4.470	-1.750	13.2	11.4	17.6
26.00	5653.870	4.390	-1.540	29.4	26.3	35.7
26.00	5661.348	4.280	-1.760	16.4	12.8	21.9
26.00	5679.023	4.650	-0.750	49.7	45.8	58.0
26.00	5701.544	2.560	-2.160	77.1	69.6	82.2
26.00	5705.464	4.300	-1.360	30.9	26.2	38.1
26.00	5731.760	4.260	-1.200	49.8	44.3	56.8
26.00	5778.453	2.590	-3.440	17.8	13.4	21.9
26.00	5784.660	3.400	-2.530	19.5	15.7	27.8
26.00	5793.914	4.220	-1.620	27.1	21.7	33.2
26.00	5806.730	4.610	-0.950	44.8	40.0	54.1
26.00	5809.218	3.880	-1.610	40.2	34.6	50.2
26.00	5852.220	4.550	-1.230	31.6	27.8	40.4
26.00	5855.076	4.610	-1.480	15.9	13.0	23.0
26.00	5859.590	4.550	-0.580	63.4	58.4	72.5
26.00	5905.672	4.650	-0.690	48.6	44.4	58.6
26.00	5916.247	2.450	-2.940	46.7	39.8	54.2
26.00	5927.789	4.650	-1.040	32.9	30.4	41.9
26.00	5929.680	4.550	-1.310	31.2	28.0	39.4
26.00	5934.655	3.930	-1.070	67.8	61.0	75.6
26.00	5956.694	0.860	-4.610	42.6	36.6	52.6
26.00	6005.541	2.590	-3.430	15.9	12.6	22.1
26.00	6024.058	4.550	-0.020	97.6	92.4	110.1
26.00	6027.050	4.080	-1.090	56.1	51.8	63.2
26.00	6056.005	4.730	-0.400	63.9	59.4	71.5
26.00	6065.482	2.610	-1.530	109.1	101.5	117.7
26.00	6079.009	4.650	-1.020	37.1	32.4	46.5
26.00	6082.711	2.220	-3.570	27.9	22.3	34.5
26.00	6093.644	4.610	-1.300	24.7	19.7	31.3
26.00	6096.665	3.980	-1.810	30.0	24.6	36.5
26.00	6127.910	4.140	-1.400	39.7	36.1	50.5
26.00	6151.618	2.180	-3.280	42.0	36.4	50.2
26.00	6165.360	4.140	-1.460	36.8	31.7	45.6
26.00	6170.510	4.800	-0.380	67.8	62.0	80.0
26.00	6173.335	2.220	-2.880	61.1	55.1	68.5
26.00	6187.990	3.940	-1.620	38.9	33.7	48.0
26.00	6200.313	2.610	-2.420	65.6	58.6	71.2
26.00	6213.430	2.220	-2.520	76.3	69.5	82.9
26.00	6219.281	2.200	-2.430	82.3	76.3	88.7
26.00	6226.736	3.880	-2.100	21.8	18.4	30.2
26.00	6229.230	2.850	-2.830	29.8	26.1	40.3
26.00	6240.646	2.220	-3.290	39.7	34.7	50.2
26.00	6252.555	2.400	-1.690	112.1	103.5	120.6
26.00	6265.134	2.180	-2.550	78.5	72.8	86.7
26.00	6270.225	2.860	-2.540	43.2	38.4	51.9
26.00	6271.279	3.330	-2.700	19.1	14.3	23.1
26.00	6297.790	2.220	-2.710	66.9	61.6	75.5
26.00	6322.690	2.590	-2.430	66.9	61.9	76.0
26.00	6335.330	2.200	-2.260	89.9	82.7	95.4

Table 1. Continued.

Element	λ [Å]	EP [eV]	$\log gf$ [dex]	EW_1 [mÅ]	EW_2 [mÅ]	EW_{Sun} [mÅ]
26.00	6336.820	3.690	-0.930	99.4	89.4	105.4
26.00	6344.150	2.430	-2.920	51.0	44.3	59.3
26.00	6380.743	4.190	-1.320	43.6	38.6	52.9
26.00	6392.539	2.280	-4.030	13.0	9.0	16.8
26.00	6419.950	4.730	-0.240	74.7	68.3	85.0
26.00	6430.846	2.180	-2.010	104.9	96.0	112.1
26.00	6481.870	2.280	-2.980	55.8	49.3	64.6
26.00	6498.939	0.960	-4.700	37.1	31.3	46.8
26.00	6518.370	2.830	-2.450	47.7	42.8	56.8
26.00	6574.229	0.990	-5.010	22.8	16.6	29.0
26.00	6593.871	2.430	-2.390	75.5	70.2	84.2
26.00	6597.561	4.800	-0.970	34.8	31.9	43.3
26.00	6609.110	2.560	-2.680	58.1	50.9	65.3
26.00	6677.987	2.690	-1.420	117.7	107.4	123.6
26.00	6703.567	2.760	-3.020	28.7	24.8	36.3
26.00	6713.745	4.800	-1.400	15.4	12.5	20.1
26.00	6725.357	4.100	-2.190	12.2	10.5	18.2
26.00	6726.667	4.610	-1.030	37.8	34.0	48.5
26.00	6733.151	4.640	-1.470	19.0	16.8	25.9
26.00	6750.152	2.420	-2.620	67.3	61.0	72.9
26.00	6752.707	4.640	-1.200	27.8	23.3	36.5
26.00	6806.845	2.730	-3.110	27.0	21.3	33.1
26.00	6810.263	4.610	-0.990	41.6	35.9	51.2
26.00	6837.006	4.590	-1.690	13.6	10.9	19.0
26.00	6839.830	2.560	-3.350	23.1	17.6	31.1
26.00	6842.690	4.640	-1.220	29.7	24.7	37.3
26.00	6843.656	4.550	-0.830	51.2	46.4	59.7
26.00	6858.150	4.610	-0.940	42.4	38.3	51.3
26.10	4491.400	2.860	-2.660	67.5	68.3	76.3
26.10	4508.290	2.860	-2.520	77.5	79.9	84.4
26.10	4520.220	2.810	-2.650	72.8	74.1	78.2
26.10	4576.330	2.840	-2.950	55.2	56.1	62.8
26.10	4620.510	2.830	-3.210	42.5	44.3	50.8
26.10	4993.340	2.810	-3.730	29.5	31.1	38.5
26.10	5132.660	2.810	-4.170	15.5	16.5	24.1
26.10	5197.577	3.230	-2.220	72.8	74.7	80.4
26.10	5264.812	3.230	-3.130	35.1	38.3	45.0
26.10	5414.073	3.220	-3.580	19.4	20.0	25.1
26.10	5425.257	3.200	-3.220	31.6	33.4	41.0
26.10	6084.111	3.200	-3.830	14.4	15.9	19.9
26.10	6149.240	3.890	-2.750	27.7	29.7	35.9
26.10	6238.380	3.890	-2.630	34.2	35.4	44.0
26.10	6369.462	2.890	-4.110	13.3	13.9	18.2
26.10	6416.919	3.890	-2.750	31.9	33.4	40.2
26.10	6432.680	2.890	-3.570	32.7	33.5	40.1
26.10	6456.383	3.900	-2.050	53.2	55.8	61.4
27.00	4792.492	4.069	-2.360			
27.00	4792.846	3.250	-0.070			
27.00	4812.967	4.229	-3.750			
27.00	4813.006	4.172	-3.440			
27.00	4813.449	2.868	-2.120			
27.00	4813.467	3.213	0.050			
27.00	4813.794	2.872	-3.410			
27.00	4813.966	3.295	-1.040			
27.00	4814.042	2.628	-4.740			
27.00	5212.691	3.512	-0.110			
27.00	5213.316	4.471	-3.230			
27.00	5301.039	1.709	-2.000			
27.00	5301.101	2.135	-1.750			
27.00	5483.344	1.709	-1.490			

Table 1. Continued.

Element	λ [Å]	EP [eV]	$\log gf$ [dex]	EW_1 [mÅ]	EW_2 [mÅ]	EW_{Sun} [mÅ]
27.00	5483.374	4.501	-3.790			
27.00	5483.955	3.629	-0.480			
27.00	5647.107	4.146	-2.340			
27.00	5647.234	2.278	-1.560			
27.00	6093.143	1.739	-2.440			
27.00	6454.990	3.629	-0.250			
28.00	4831.180	3.610	-0.320	66.1	63.2	73.2
28.00	4866.270	3.540	-0.210	70.3	65.2	69.7
28.00	4904.420	3.540	-0.250	80.8	77.6	87.1
28.00	4913.980	3.740	-0.660	46.6	43.7	55.9
28.00	4946.040	3.800	-1.220	20.0	15.6	26.0
28.00	4952.290	3.610	-1.260	24.7	21.4	32.1
28.00	4953.208	3.740	-0.660	46.8	43.7	54.6
28.00	4976.135	3.610	-1.250	21.3	18.0	30.6
28.00	4998.220	3.610	-0.690	48.2	43.4	68.3
28.00	5010.938	3.640	-0.870	41.7	37.2	47.9
28.00	5082.350	3.660	-0.590	59.1	53.7	66.4
28.00	5084.110	3.680	-0.060	83.6	78.9	88.0
28.00	5088.960	3.680	-1.290	21.4	17.5	24.6
28.00	5094.420	3.830	-1.070	22.9	19.8	28.2
28.00	5102.970	1.680	-2.660	41.2	36.5	49.2
28.00	5157.980	3.610	-1.510	13.1	12.2	18.6
28.00	5176.560	3.900	-0.440	46.8	44.0	54.5
28.00	5392.330	4.150	-1.320	9.5	7.9	12.5
28.00	5578.729	1.680	-2.570	47.1	41.5	55.0
28.00	5587.870	1.930	-2.440	44.6	40.0	53.5
28.00	5589.358	3.900	-1.140	19.8	18.0	25.9
28.00	5593.746	3.900	-0.780	33.4	30.4	43.5
28.00	5625.320	4.090	-0.730	29.4	26.4	36.3
28.00	5628.350	4.090	-1.320	10.9	8.7	14.6
28.00	5638.750	3.900	-1.700	5.3	4.3	10.4
28.00	5641.880	4.110	-1.020	17.6	14.2	21.6
28.00	5643.078	4.160	-1.250	10.9	8.9	14.5
28.00	5694.990	4.090	-0.630	34.3	30.2	42.6
28.00	5748.360	1.680	-3.240	20.6	17.4	28.2
28.00	5754.670	1.930	-1.850	65.4	61.2	73.6
28.00	5805.217	4.170	-0.640	33.0	28.5	40.0
28.00	5847.010	1.676	-3.410	17.1	13.2	22.5
28.00	5996.740	4.236	-1.010	13.8	12.9	20.4
28.00	6007.317	1.677	-3.410	17.7	15.6	25.1
28.00	6086.282	4.270	-0.510	34.0	28.9	43.8
28.00	6108.116	1.680	-2.440	53.2	48.4	66.8
28.00	6111.080	4.088	-0.810	26.3	23.6	34.1
28.00	6119.760	4.270	-1.316	7.5	6.2	10.5
28.00	6128.984	1.677	-3.360	19.1	16.1	26.2
28.00	6130.135	4.270	-0.960	14.2	12.2	21.9
28.00	6175.370	4.089	-0.550	39.5	37.0	49.5
28.00	6176.811	4.090	-0.260	53.7	50.3	65.4
28.00	6177.242	1.830	-3.510	10.2	9.4	15.3
28.00	6186.717	4.110	-0.960	23.6	18.4	31.3
28.00	6204.604	4.090	-1.140	16.3	13.9	22.7
28.00	6223.971	4.105	-1.466	20.9	17.3	29.2
28.00	6230.100	4.110	-1.132	13.8	11.9	21.2
28.00	6322.169	4.154	-1.210	12.2	9.1	18.0
28.00	6327.600	1.680	-3.060	28.2	22.7	37.9
28.00	6360.810	4.170	-1.150	12.7	12.6	16.5
28.00	6378.233	4.154	-1.386	22.0	20.8	31.6
28.00	6482.810	1.930	-2.760	50.8	49.0	39.6
28.00	6598.611	4.236	-0.910	17.0	15.6	25.1
28.00	6635.130	4.420	-0.720	17.3	14.8	23.8

Table 1. Continued.

Element	λ [Å]	EP [eV]	$\log gf$ [dex]	EW_1 [mÅ]	EW_2 [mÅ]	EW_{Sun} [mÅ]
28.00	6643.630	1.680	-2.000	84.5	77.5	94.8
28.00	6767.772	1.830	-2.170	71.1	66.1	80.2
28.00	6772.315	3.660	-0.990	37.9	36.0	50.9
28.00	6842.043	3.658	-1.500	19.1	17.0	23.4
29.00	5218.197	3.814	0.480			
30.00	4722.159	4.030	-0.380	64.6	65.2	69.6
30.00	4810.534	4.080	-0.160	67.7	68.2	74.3
30.00	6362.350	5.790	0.140	14.9	16.0	19.8
38.00	4607.338	0.000	0.283	37.2	29.8	45.7
38.10	4161.800	2.940	-0.500	19.4	19.0	25.7
39.10	4854.867	0.992	-0.380	36.4	35.3	43.8
39.10	4883.685	1.084	0.070	48.7	48.0	56.3
39.10	4900.110	1.033	-0.090	44.0	45.0	54.6
39.10	5200.413	0.992	-0.570	26.9	27.0	36.7
40.10	4050.320	0.713	-1.060	18.5	14.5	22.3
40.10	4208.980	0.713	-0.510	37.0	38.0	42.9
56.10	5853.696	0.604	-2.915	56.4	54.8	63.0
56.10	6141.697	0.704	-2.495	112.1	104.3	115.6
56.10	6496.900	0.604	-2.000	94.1	93.3	98.7
56.10	5853.686	0.604	-2.066			
56.10	5853.687	0.604	-2.066			
56.10	5853.687	0.604	-2.009			
56.10	5853.688	0.604	-2.009			
56.10	5853.689	0.604	-2.215			
56.10	5853.689	0.604	-2.215			
56.10	5853.690	0.604	-1.010			
56.10	5853.690	0.604	-1.466			
56.10	5853.690	0.604	-1.914			
56.10	5853.690	0.604	-2.620			
56.10	5853.690	0.604	-1.010			
56.10	5853.690	0.604	-1.466			
56.10	5853.690	0.604	-1.914			
56.10	5853.690	0.604	-2.620			
56.10	5853.690	0.604	-1.010			
56.10	5853.691	0.604	-2.215			
56.10	5853.692	0.604	-2.215			
56.10	5853.693	0.604	-2.009			
56.10	5853.693	0.604	-2.009			
56.10	5853.694	0.604	-2.066			
56.10	5853.694	0.604	-2.066			
56.10	6141.725	0.704	-2.456			
56.10	6141.725	0.704	-2.456			
56.10	6141.727	0.704	-1.311			
56.10	6141.727	0.704	-1.311			
56.10	6141.728	0.704	-2.284			
56.10	6141.728	0.704	-2.284			
56.10	6141.729	0.704	-0.503			
56.10	6141.729	0.704	-1.214			
56.10	6141.729	0.704	-0.503			
56.10	6141.729	0.704	-1.214			
56.10	6141.730	0.704	-0.077			
56.10	6141.730	0.704	-0.077			
56.10	6141.730	0.704	-0.077			
56.10	6141.731	0.704	-0.709			
56.10	6141.731	0.704	-1.327			
56.10	6141.731	0.704	-0.709			
56.10	6141.731	0.704	-1.327			
56.10	6141.732	0.704	-0.959			
56.10	6141.732	0.704	-1.281			
56.10	6141.732	0.704	-0.959			

Table 1. Continued.

Element	λ [Å]	EP [eV]	$\log gf$ [dex]	EW_1 [mÅ]	EW_2 [mÅ]	EW_{Sun} [mÅ]
56.10	6141.733	0.704	-1.281			
56.10	6496.898	0.604	-1.886			
56.10	6496.899	0.604	-1.886			
56.10	6496.901	0.604	-1.186			
56.10	6496.902	0.604	-1.186			
56.10	6496.906	0.604	-0.739			
56.10	6496.906	0.604	-0.739			
56.10	6496.910	0.604	-0.380			
56.10	6496.910	0.604	-0.380			
56.10	6496.910	0.604	-0.380			
56.10	6496.916	0.604	-1.583			
56.10	6496.916	0.604	-1.583			
56.10	6496.917	0.604	-1.186			
56.10	6496.918	0.604	-1.186			
56.10	6496.920	0.604	-1.186			
56.10	6496.922	0.604	-1.186			
57.10	4662.500	0.000	-1.240	7.3	6.2	5.7
58.10	4042.581	0.495	0.000	7.8	7.9	11.0
58.10	4073.474	0.477	0.210	13.7	12.8	39.5
58.10	4364.653	0.495	-0.170	8.8	9.2	11.5
58.10	4523.075	0.516	-0.080	11.2	10.5	13.8
58.10	4562.359	0.477	0.210	20.0	18.4	22.2
58.10	5274.229	1.044	0.130	5.9	5.7	7.5
60.10	4021.330	0.320	-0.100	10.5	10.8	5.7
60.10	4446.380	0.204	-0.350	7.7	7.8	5.6
63.10	4129.720	0.000	0.220	46.2	46.7	55.5
64.10	4251.731	0.382	-0.220	8.8	7.7	14.0
66.10	4077.970	0.103	-0.040	31.6	26.0	27.4
66.10	4103.310	0.103	-0.380	9.8	10.4	13.1
66.10	4449.700	0.000	-1.030	5.0	4.1	3.8

Table 3. Differential abundances for the stars ζ^1 Ret and ζ^2 Ret relative to the Sun, and ζ^1 Ret relative to ζ^2 Ret. We also present the observational errors σ_{obs} , errors due to stellar parameters σ_{par} , as well as the total error σ_{TOT} .

Element	[X/Fe]	(ζ^1 Ret - Sun)				(ζ^2 Ret - Sun)				(ζ^1 Ret - ζ^2 Ret)			
		σ_{obs}	σ_{par}	σ_{TOT}	[X/Fe]	σ_{obs}	σ_{par}	σ_{TOT}	[X/Fe]	σ_{obs}	σ_{par}	σ_{TOT}	
[C I/Fe]	0.050	0.060	0.047	0.076	0.051	0.060	0.021	0.064	0.000	0.040	0.018	0.044	
[O I/Fe]	-0.045	0.049	0.023	0.054	0.095	0.054	0.020	0.057	-0.139	0.005	0.016	0.017	
[Na I/Fe]	0.004	0.040	0.010	0.041	0.009	0.016	0.009	0.018	-0.003	0.026	0.007	0.027	
[Mg I/Fe]	0.110	0.044	0.019	0.048	0.133	0.039	0.010	0.040	-0.022	0.011	0.008	0.014	
[Al I/Fe]	0.060	0.028	0.011	0.030	0.007	0.058	0.010	0.059	0.054	0.034	0.008	0.035	
[Si I/Fe]	0.024	0.012	0.002	0.014	0.045	0.012	0.002	0.013	-0.020	0.005	0.001	0.006	
[S I/Fe]	0.096	0.103	0.021	0.105	0.176	0.048	0.017	0.051	-0.080	0.054	0.014	0.056	
[Ca I/Fe]	0.074	0.008	0.011	0.015	0.067	0.011	0.006	0.012	0.008	0.006	0.005	0.008	
[Sc I/Fe]	0.083	0.070	0.028	0.076	0.075	0.003	0.026	0.026	0.009	0.073	0.021	0.076	
[Sc II/Fe]	0.003	0.017	0.025	0.031	-0.011	0.018	0.011	0.021	0.015	0.002	0.008	0.009	
[Ti I/Fe]	0.085	0.008	0.008	0.012	0.070	0.009	0.005	0.011	0.016	0.006	0.004	0.007	
[Ti II/Fe]	0.051	0.014	0.016	0.021	0.060	0.011	0.006	0.013	-0.008	0.008	0.005	0.010	
[V I/Fe]	-0.236	0.016	0.014	0.022	-0.278	0.017	0.006	0.019	0.044	0.008	0.005	0.010	
[Cr I/Fe]	0.031	0.010	0.009	0.014	0.034	0.012	0.005	0.013	-0.002	0.008	0.004	0.010	
[Cr II/Fe]	0.047	0.016	0.022	0.028	0.045	0.016	0.009	0.019	0.003	0.022	0.007	0.023	
[Mn I/Fe]	-0.369	0.067	0.024	0.071	-0.285	0.022	0.011	0.024	0.043	0.023	0.009	0.024	
[Co I/Fe]	-0.155	0.011	0.018	0.022	-0.173	0.010	0.008	0.013	0.018	0.015	0.007	0.017	
[Ni I/Fe]	-0.006	0.010	0.004	0.012	0.005	0.011	0.002	0.012	-0.010	0.005	0.002	0.006	
[Cu I/Fe]	-0.185	0.060	0.047	0.076	-0.215	0.060	0.021	0.064	0.031	0.040	0.018	0.044	
[Zn I/Fe]	0.041	0.013	0.044	0.046	0.068	0.013	0.010	0.016	-0.025	0.010	0.010	0.015	
[Sr I/Fe]	-0.053	0.060	0.078	0.099	-0.110	0.060	0.031	0.067	0.058	0.040	0.030	0.050	
[Sr II/Fe]	0.008	0.060	0.032	0.068	-0.005	0.060	0.017	0.062	0.014	0.040	0.013	0.042	
[Y II/Fe]	-0.050	0.026	0.049	0.056	-0.057	0.012	0.014	0.019	0.007	0.017	0.014	0.022	
[Zr II/Fe]	0.042	0.025	0.060	0.066	0.003	0.074	0.022	0.077	0.040	0.099	0.019	0.101	
[Ba II/Fe]	-0.095	0.065	0.033	0.073	-0.208	0.057	0.015	0.059	0.114	0.022	0.013	0.026	
[La II/Fe]	0.287	0.060	0.027	0.066	0.261	0.060	0.023	0.064	0.027	0.040	0.015	0.043	
[Ce II/Fe]	-0.073	0.134	0.014	0.134	-0.047	0.137	0.009	0.137	-0.035	0.016	0.006	0.018	
[Nd II/Fe]	0.399	0.112	0.028	0.116	0.468	0.115	0.022	0.117	-0.068	0.003	0.015	0.016	
[Eu II/Fe]	-0.110	0.060	0.200	0.209	-0.133	0.060	0.040	0.072	0.024	0.040	0.054	0.067	
[Gd II/Fe]	-0.079	0.060	0.027	0.066	-0.100	0.060	0.022	0.064	0.022	0.040	0.014	0.043	
[Dy II/Fe]	0.211	0.124	0.035	0.129	0.174	0.057	0.016	0.060	0.037	0.088	0.014	0.090	

